Detection of Limestone Cavities Using Geophysical Techniques

J. Tiah and C. Veeresh

Land Transport Authority, Singapore

ABSTRACT:

Rapid urbanisation in Singapore necessitates underground infrastructure, particularly in the western areas, where limestone formations with karst features and cavities are found to exists. These cavities pose serious challenges to construction work. Bored tunnelling through limestone cavities may result in the formation of sinkholes and blowouts. Therefore, early detection and treatment of cavities is essential for safe construction. While borehole drilling provides accurate cavity detection, its limited coverage leaves ground conditions between boreholes uncertain. Geophysical investigations offer broader area scanning to identify high-risk zones. There are several geophysical methods available with varying degrees of accuracy but identifying a suitable method is a challenging task when it comes to detecting limestone cavities. This paper assesses the effectiveness of various geophysical methods to help engineers choose suitable techniques for safe tunnelling in such complex ground conditions.

1. INTRODUCTION

Upcoming rail construction such as the cross island line (CRL) and other underground projects are expected to encounter limestone which is prone to have karst features. Karst processes often result from underground natural cavities due to the erosive effect of groundwater, known as dissolution, on carbonate rocks. The presence of cavities in limestone poses a potential risk during the construction phase as well as in the long term if it is not detected and treated. In terms of bored tunnelling, the presence of cavities may cause face pressure loss resulting in sink holes or blow outs.

Reliable site investigation is essential for detecting the presence of cavities. Investigation methods can be categorised as intrusive and non-intrusive. A common intrusive method for ground investigation is drilling a borehole or probe hole. The detection of cavities is very challenging along the tunnel alignment as the boreholes are only 10mm in diameter and drilled at a spacing. Information between the boreholes remains unknown and limestone cavities may go undetected. Due to the limitation of the physical drilling method of detection, geophysical survey which was studied and explored by early pioneers (Reyleigh 1985, Love 2013, Lamb 1904) can provide indication of locations with high potential of cavities and guide engineers on locations to probe for further investigation of limestone cavities.

Geophysical methods are broadly categorized into 4 types – seismic, electrical resistivity, magnetic and gravity and are summarized as follows: 1) seismic survey uses the propagation of elastic waves to measure the velocities in different material 2) resistivity survey detects variation in electrical resistivity in the subsurface 3) magnetic survey detects magnetic field variations which is primarily used to locate metal deposits and 4) gravity survey assesses density variation across the subsurface to determine localized geological features. Cavities often occur in carbonate rocks like limestone which have low magnetic susceptibility (Elhaj 2015, Krasnoperov et al 2023). Therefore, the contrast between the cavities and surrounding rock is too small to be detected magnetically. For the electrical resistivity method, in a highly urbanized city like Singapore, electrical noise from power lines, underground utilities, MRT tunnels and buildings can distort resistivity data and electromagnetic interference. Further, shallow water table and high content of clay rich soil (Sangprasat, 2025) reduce resistivity

contrast between air filled cavities and surrounding material (Coulouma et al, 2000), making cavities harder to detect.

In view of the above consideration, this study will only focus on seismic and gravity methods for the detection of cavity. This paper reviews the study of four different types of geophysical methods carried out at the same site. They are (1) Microgravity Survey, (2) Crosshole Seismic Tomography, (3) Microtremor (MAM) and (4) Seismic Scattering. Details of the methods and results are discussed in the following sections.

2. DESCRIPTION AND GEOLOGY OF STUDY AREA

The test site is located at the western area of Singapore as shown in Figure 2. The geology is predominantly in Pandan formation of the Jurong Group.

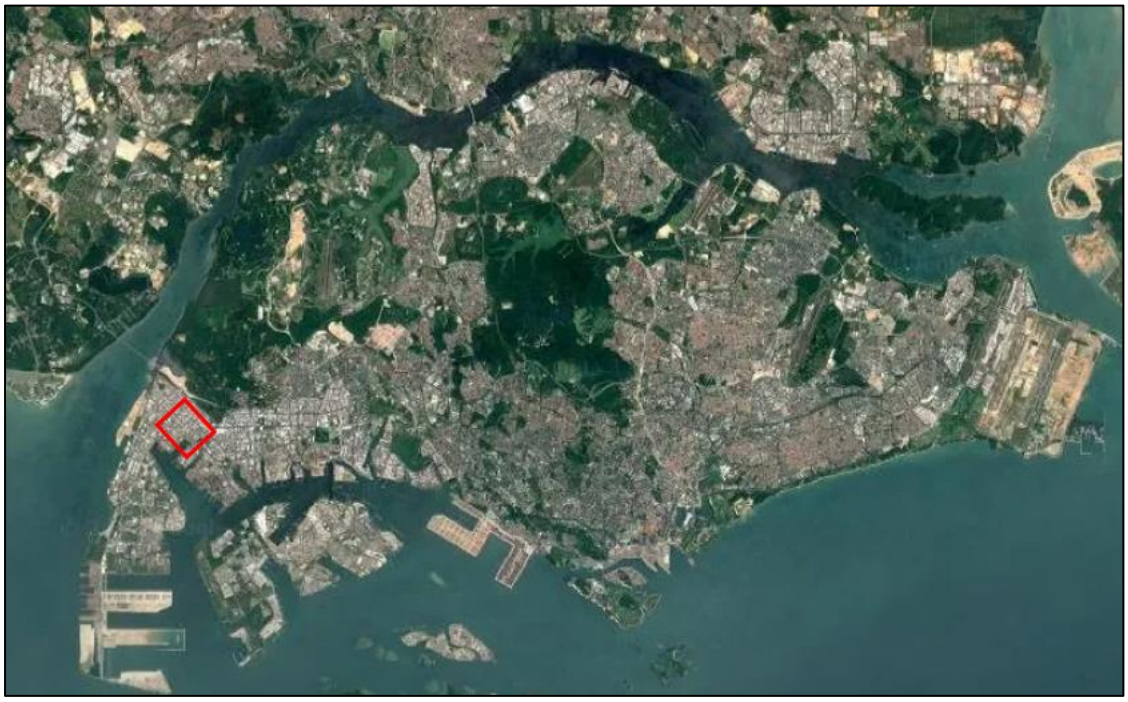

Figure 2: Test Site

Based on data from approximately 2165 numbers of boreholes in the western part of Singapore, presence of limestone and limestone cavities occurrence in the different Jurong Group is summarised in Table 2. From this data, it is noted that Pandan formation exhibit higher chance of encountering limestone cavities followed by Boon Lay formation and lastly, Ayer Chawan formation.

Jurong Group	% of BHs with limestone occurrence	% of BHs with cavity occurrence
Pandan Formation	34.0	4.3
Boon Lay Formation	11.3	0.5
Ayer Chawan Formation	2.6	0.2

Table 2: % of limestone and cavity occurrence in the different types of Jurong Group

Similar trends are observed from BCA (2021) geological map as shown in Figure 3.

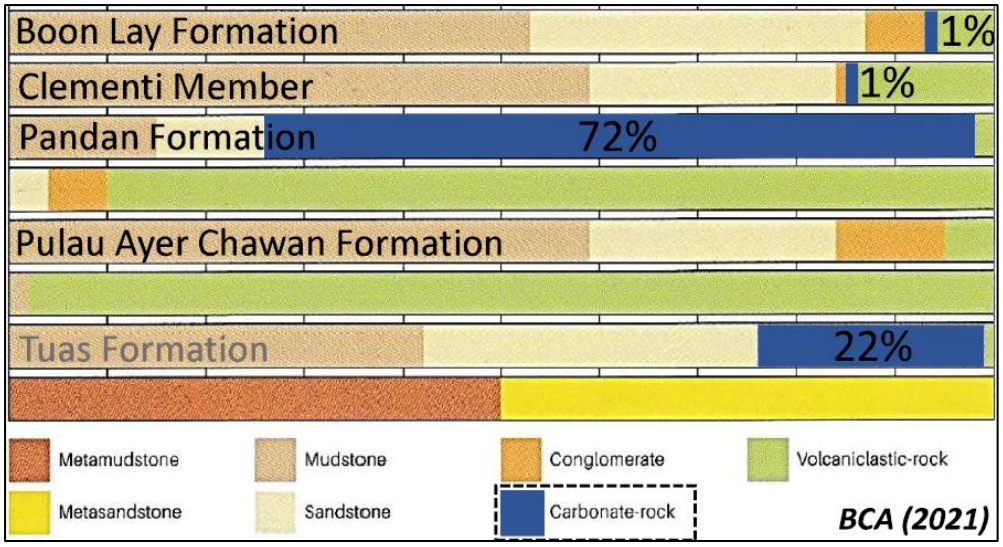

Figure 3: BCA deep ground investigation programme (2021)

Various methods described in section 1 are tested in Pandan formation and details of different tests are presented in the following section.

3. INVESTIGATION METHODS

3.1 Microgravity Survey

The microgravity technique in civil engineering involves measuring tiny variations in Earth's gravity to detect underground voids and cavities. These small gravity anomalies are difficult to detect due to larger variations caused by factors like height, latitude and geology. Advances in high-resolution equipment and analysis methods have improved detection and interpretation of these anomalies, providing information on the location, shape, and size of voids without disturbing the ground. The technique is increasingly used in engineering to identify natural and man-made cavities (Bishop, 1997). Gravity changes are measured in very small units called microgals, as the typical gravitational acceleration (around 9.8 m/s^2) is too large for detecting such subtle variations.

A gravimeter, shown in Figure 3.1, a highly precise instrument using a spring and a proof mass, is used to measure the gravity value at a point. Based on the mass displacement and the changes in the length of the spring, gravity value can be calculated. As shown in Figure 3.2, the principle of a gravity survey is straightforward: areas with low-density materials underground, like cavities or caves, cause a relatively low gravity anomaly, while denser materials cause higher anomalies. In gravity surveys, the microgravity anomalies from shallow density changes (the target) are often hidden within larger regional gravity anomalies caused by deeper structures. Therefore, filtering techniques are needed to isolate the target microgravity anomalies from the overall gravity data.

Figure 3.1 Set up of a gravimeter

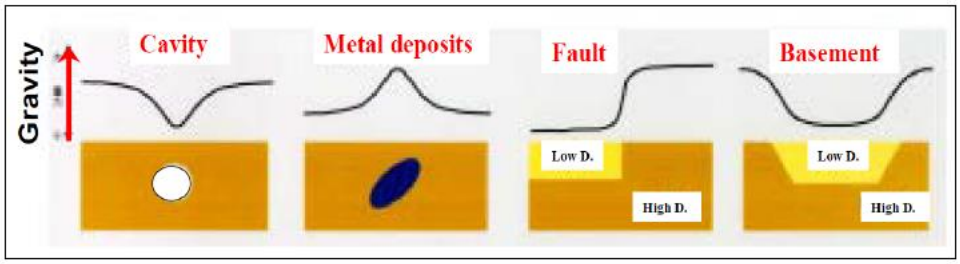

Figure 3.2 Illustrations showing relative surface variation of Earth's gravitational acceleration over geologic structures.

The study uses the loop method for gravity measurements, starting and ending at a Base Station (BS) with several intermediate stations in between. Measuring gravity twice at the base station helps correct for instrumental drift. Each measurement loop takes about 4 to 5 hours to complete. Microgravity data are collected at stations arranged in a survey grid that extends beyond the area of interest to include background conditions. Station spacing, typically around 5 meters, is planned based on the target depth. As microgravity data are highly sensitive to elevation changes, station elevations must be measured with about 3mm precision. The survey uses high-resolution gravimeters with a resolution of 10 microgals.

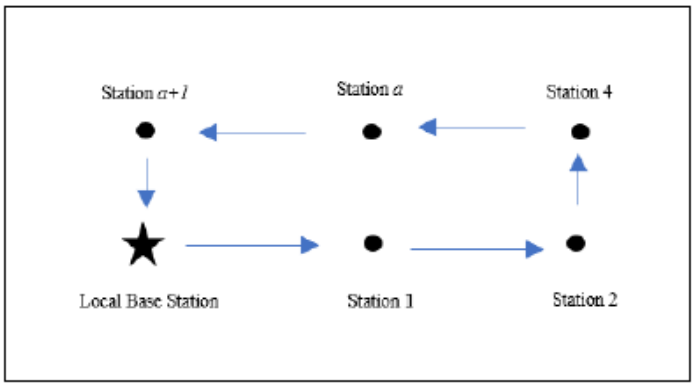

Figure 3.3 Loop Method

Raw gravity data from field measurements include erroneous factors to be corrected such as gravitational pull of the Sun and Moon (Earth tides), topographic mass effects, and variations in distance

from Earth's center (height effect). Gravity data is qualitatively examined and interpolated to identify lateral variations. Additional survey points are added around significant anomalies to improve resolution.

3.2 Crosshole Tomography

Crosshole-seismic tomography aims to detect anomalies or cavities and map soil or rock layers between boreholes. Tomography involves iteratively inverting a matrix of material properties to create a cross-sectional image at a region (William 1999). As shown in Figure 3.4, in crosshole-seismic tomography, an acoustic source in one borehole and a receiver in another measure compressional wave arrival times. These times reflect the material properties between the boreholes. Variations in seismic velocity indicate differences in subsurface features like weathered bedrock, fractures, voids, or solution zones. The resulting image, called a tomogram, shows the internal velocity structure based on wave paths from multiple angles.

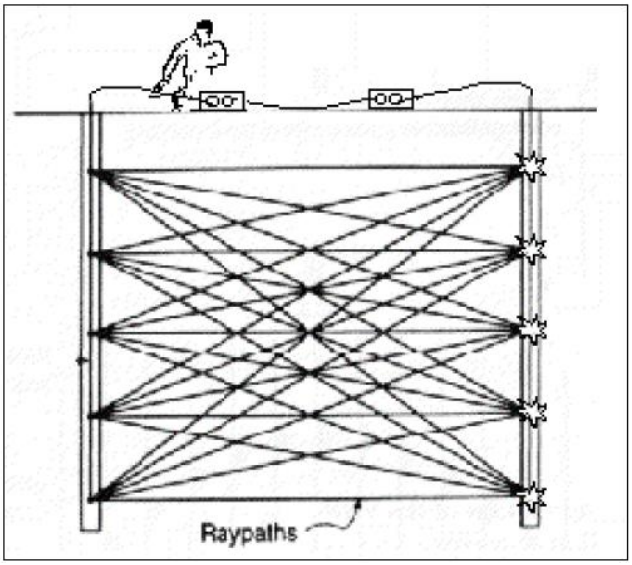

Figure 3.4 Schematic of Crosshole seismic tomography and ray paths

Twenty-four hydrophones (Figure 3.6) spaced at 1m are installed in the top 24 meters of the receiver borehole, while a sparker (Figure 3.5) serves as the seismic source in a separate borehole. Shots start at the bottom of the source borehole using low power, increasing power if waveforms are unclear or noisy. After each shot, the sparker is moved up by 1 meter until it reaches the top. It is crucial that the boreholes remain filled with water throughout the survey.

Figure 3.5 Lowering of Sparker

Figure 3.6 Lowering of Hydrophones

The operator sets the digital seismograph to record seismic data, using stacking if needed to improve quality in high noise. Seismic waves travel nearly horizontally along refractors, and hydrophones detect the refracted signals. These are amplified thousands of times, converted to digital form, and stored in memory. Once the signals are clear and satisfactory, the data is saved for further processing.

Crosshole-seismic tomography data analysis involves forward modeling with ray tracing and inversion using the Simultaneous Iterative Reconstruction Technique (SIRT). First arrival times of seismic waves between source and receiver boreholes are measured and plotted as travel-time curves (Louis 2001). The area between boreholes is divided into cells with constant but unknown velocities. The basic equation of forward modelling for ray equation analysis:

$$\mathbf{Ms = t}$$

Given the travel times vector t and the ray paths matrix M, we must solve for the slowness vector s. The number of rows of M equals the number of rays (first-arrival time picks). The number of columns of M equals the number of pixels (cells) in the image.

The PLOTREFA software was used to invert seismic data, offering ray tracing, inversion, grid manipulation, and display tools. Its noise-resistant algorithm calculates seismic velocity from the corrected travel time curve using Hagiwara's method to create an initial velocity model. Theoretical travel times are then iteratively recalculated and adjusted to minimize residual errors until the model accurately fits the observed data.

3.3 Microtremor

The ground surface constantly experiences low-amplitude vibrations called microtremors, caused by natural (wind, ocean waves) and artificial (traffic, factories) sources. These microtremors mainly consist of surface Rayleigh waves and have become popular in geophysics because the method is non-invasive, fast, and cost-effective. It is especially useful in complex, unconsolidated soils and can estimate deep surface wave velocity structures without needing an artificial source, with depth of investigation extended by increasing the array size (Olafsdottir, 2017).

The survey used a linear array (Figure 3.7) of up to 64 portable seismographs called Atoms (Figure 3.8), spaced 1 meter apart. Each Atom autonomously records continuous ambient noise, synchronized via GPS. Data acquisition takes about 50 minutes per array, with setup and demobilization totalling around 2 hours.

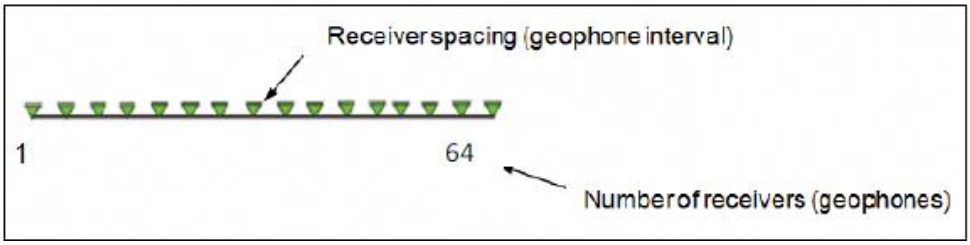

Figure 3.7 Microtremor Array – each triangle represents an ATOM

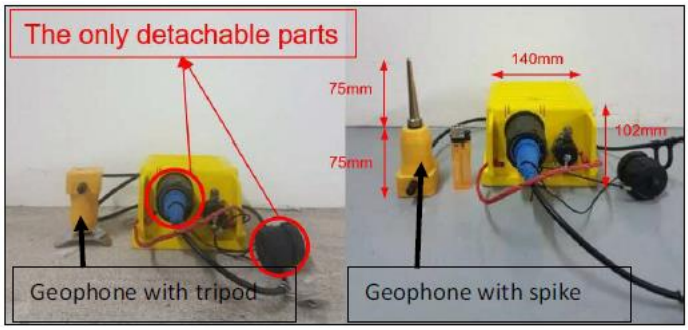

Figure 3.8 ATOM (yellow box) attached Geophone with Tripod (Left) and Geophone with Spike (Right)

Data processing applies the Common Mid-Point Spatial Auto-Correlation (CMPSPAC) method, which analyzes the vertical component of ambient noise in overlapping time blocks. Coherencies between receiver pairs are averaged in the frequency domain, and dispersion curves are derived by comparing these with theoretical models. Finally, 1D non-linear least squares inversion with horizontal constraints reconstructs pseudo 2D/3D shear wave velocity (Vs) models to characterize the subsurface.

3.4 Seismic Scattering

Seismic scattering refers to the phenomenon where seismic waves, propagating through the Earth's subsurface, interact with heterogeneities such as voids, fractures, lithological boundaries, and other discontinuities. These irregularities cause the incident seismic energy to be redistributed in multiple directions, generating scattered waves that deviate from the primary propagation path.

The scattering process arises because the subsurface is rarely homogeneous; variations in elastic properties, density, and wave velocity create perturbations in the wavefield. When an incident seismic wave encounters such a perturbation, part of its energy is reflected, refracted, or diffracted, giving rise to secondary wavefronts. The scattered wave (us) is expressed mathematically as:

$$\nabla^2 u_s - \frac{\partial^2 u_s}{v_0^2 \partial t^2} = -\frac{\alpha(x)}{v_0^2}\frac{\partial^2 u_0}{\partial t^2}$$

where the incident wave (u0), reference velocity (v0), time (t), and the perturbation parameter (α) and defined as:

$$\alpha(x) = \frac{v^2 - v_0^2}{v_0^2}$$

where v is the velocity at point x.

Seismic scattering theory leverages this principle to image subsurface features that are otherwise difficult to resolve with direct seismic arrivals. Techniques such as wavefield separation, velocity analysis, and synthetic aperture imaging utilize scattered wave data to reconstruct seismic scattering profiles (SSP), enabling the identification of small-scale anomalies like cavities, fractures, and faults. This method has been used extensively in geological and geotechnical engineering (Revenaugh, 1999; Schwenk et al., 2016), such as, to detect underground anomalies (Kesar, 2011) and buried mine-shaped anomalies (Rappaport and Miller, 1999).

The source of the waves is typically an active source such as a hitting of a hammer while the receptors are placed at 1m apart in an array along the alignment of concern and is connected to a system to analyse the scattered signals (Figure 3.9).

The detection of cavities is a notable application of seismic scattering. Cavities induce strong impedance contrasts, resulting in pronounced scattered energy. By analyzing these scattered signals, geophysicists can locate and characterize the size and shape of subsurface voids.

Figure 3.9 Set up of Seismic Scattering with receptors spaced at 1m

4. INVESTIGATION RESULTS AND DISCUSSIONS

4.1 Microgravity Survey

A microgravity survey grid of 5m by 5m spacing with a total of 48 points (101 to 148) were conducted as shown in Figure 4.2

Figure 4.1 presents the gravity anomaly results from the survey area. The data indicates slightly higher gravity values along the road, likely due to denser subsurface materials caused by past road compaction. In contrast, along the pavements adjacent to the road display lower gravity anomalies, suggesting less dense subsurface features.

At the northern corridor, several gravity points along the road pavement show pronounced lows gravity anomalies. These are interpreted to be influenced by manmade structures such as drains or box culverts, which typically contain subsurface voids or empty spaces, resulting in reduced gravitational attraction.

On the southern corridor, it appears to have two localised low gravity anomalies at points R111 and R138. To further investigate, additional gravity measurements (points N1 to N8) were collected, confirming the presence of these low anomalies. Such anomalies, especially those located in the southern corridor, are potential indicators of cavities or fractured zones.

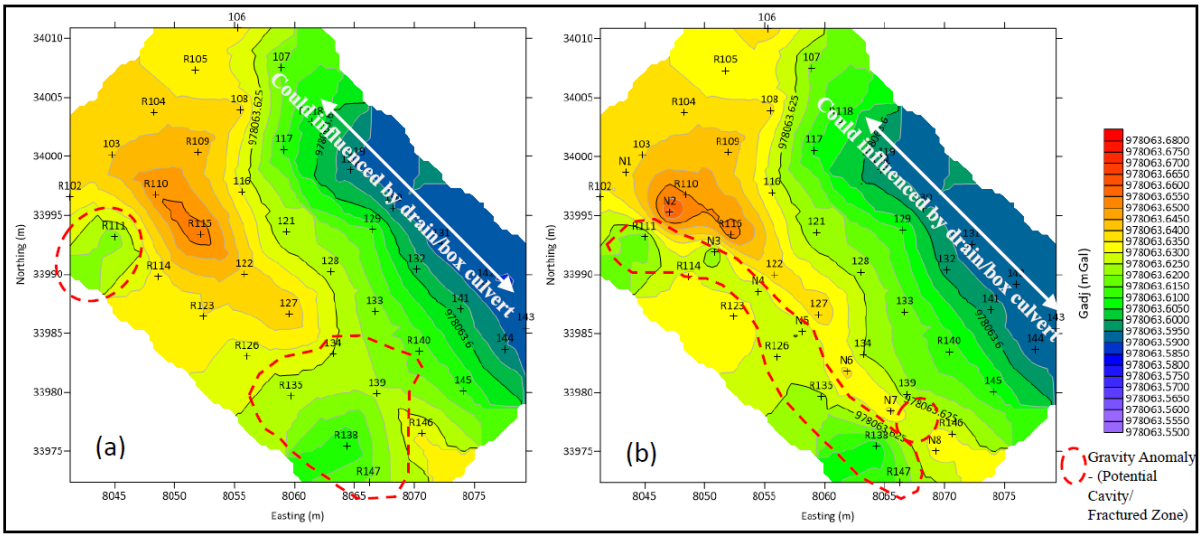

Figure 4.1 Microgravity Results

Given these findings, boreholes were carried out at these anomalous locations as shown in Figure 4.2. A schematic of the longitudinal geological profile is shown in Figure 4.3. From these results, microgravity survey is able to provide indication of presence of cavities as verified by the three boreholes RC/11288, RC/11286A and RC/11286 (Figure 4.3). Reducing the grid spacing from 5m to 2.5m between each survey points further enhance the resolution in detecting the cavities.

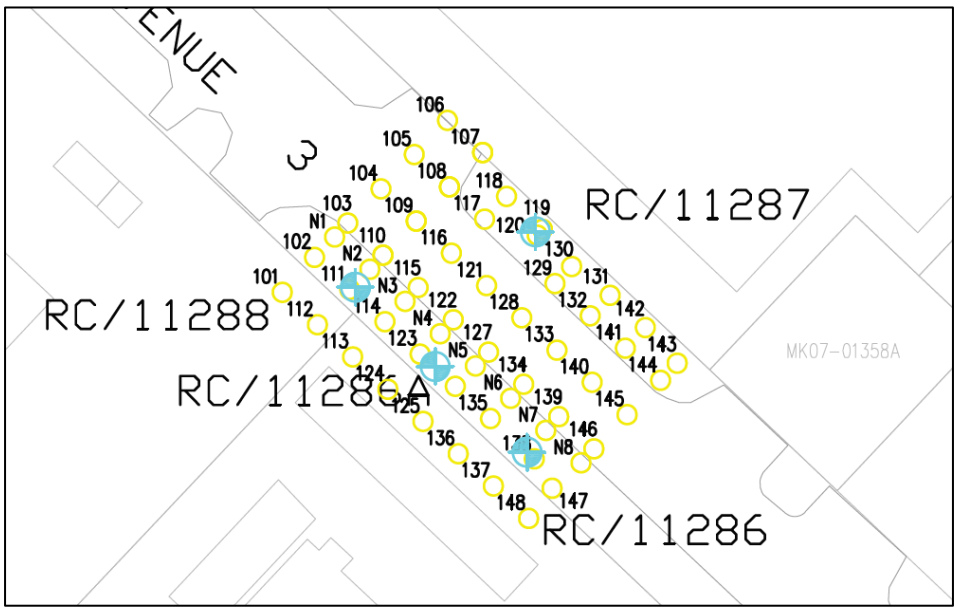

Figure 4.2 Microgravity survey points layout and borehole locations

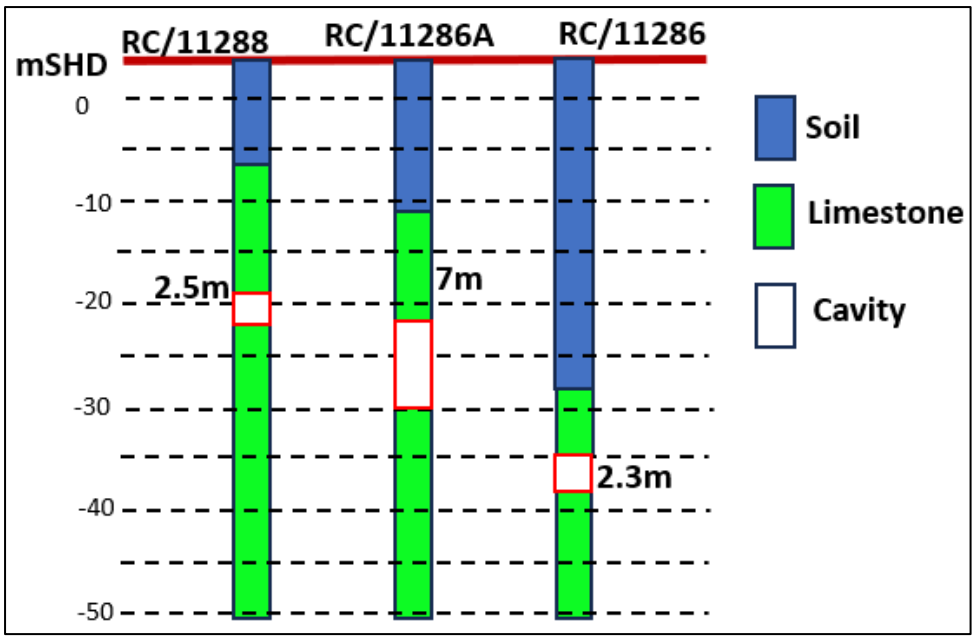

Figure 4.3 Longitudinal geological profile based on borehole logs

4.2 Crosshole Tomography

The crosshole-seismic tomography survey produced a multi-layer seismic refraction tomogram showing the geological structure of the site based on P-wave velocities, which indicate rock hardness. These velocities were correlated with known subsurface materials from the conducted borehole logs. Four crosshole tomography tests were conducted (Figure 4.4) with corresponding four profile sections are shown from Figure 4.5 and Figure 4.6 with the topographies adjusted to the Singapore Height Datum (mSHD). The geological profiles appeared relatively uniform with depth, and a summary of soil types and corresponding P-wave velocities is presented in Table 4 below.

No	Soil type	P wave velocity (m/s)
1	FILL & E	1000-1400
2	SV-SVI	1400-2400
3	SIII and better	> 2400

Table 4: Soil Type with equivalent P wave velocity

The soil profiles of the boreholes are generally consistent with the P-wave velocity ranges, showing a gradual increase in velocity with depth. Borehole data shows cavities at certain depths as shown in Figure 4.3. However, the crosshole tomography results show no indication of cavities, with the exception for the reverse direction of RC/11286A to RC/11286. This phenomenon may be attributed to the nature of the cavity being narrow and elongated, as observed from the Microgravity Survey, thus causing the ray path to travel around or along the cavity boundary. If the P-wave travels along the boundary rather than through it, the velocity may not slow down enough to capture the presence of cavity. Since P-waves travels faster in rock, no significant velocity change can be observed.

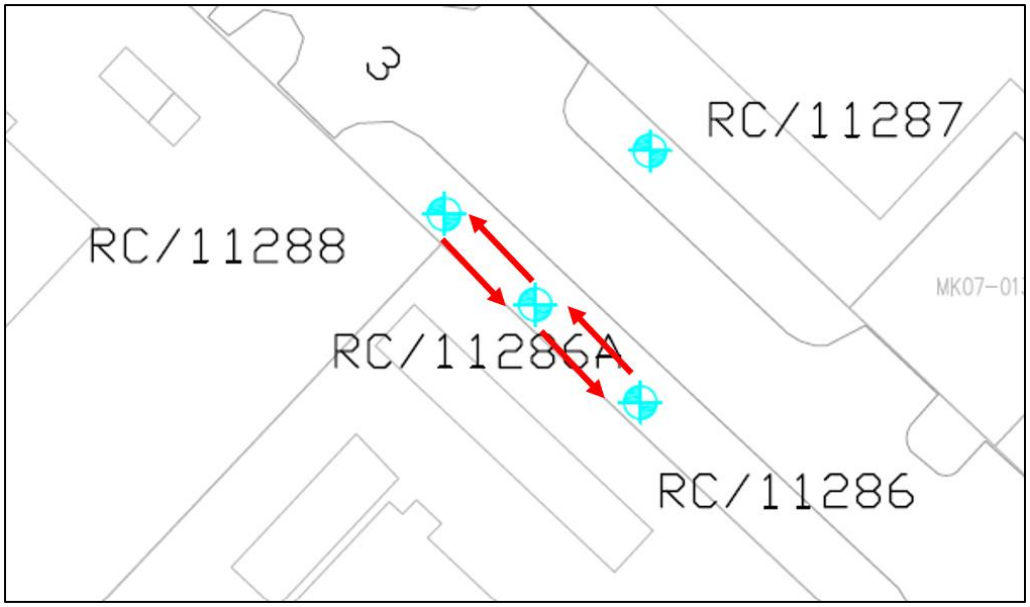

Figure 4.4 Crosshole Tomography test direction (source to receiver and reverse direction)

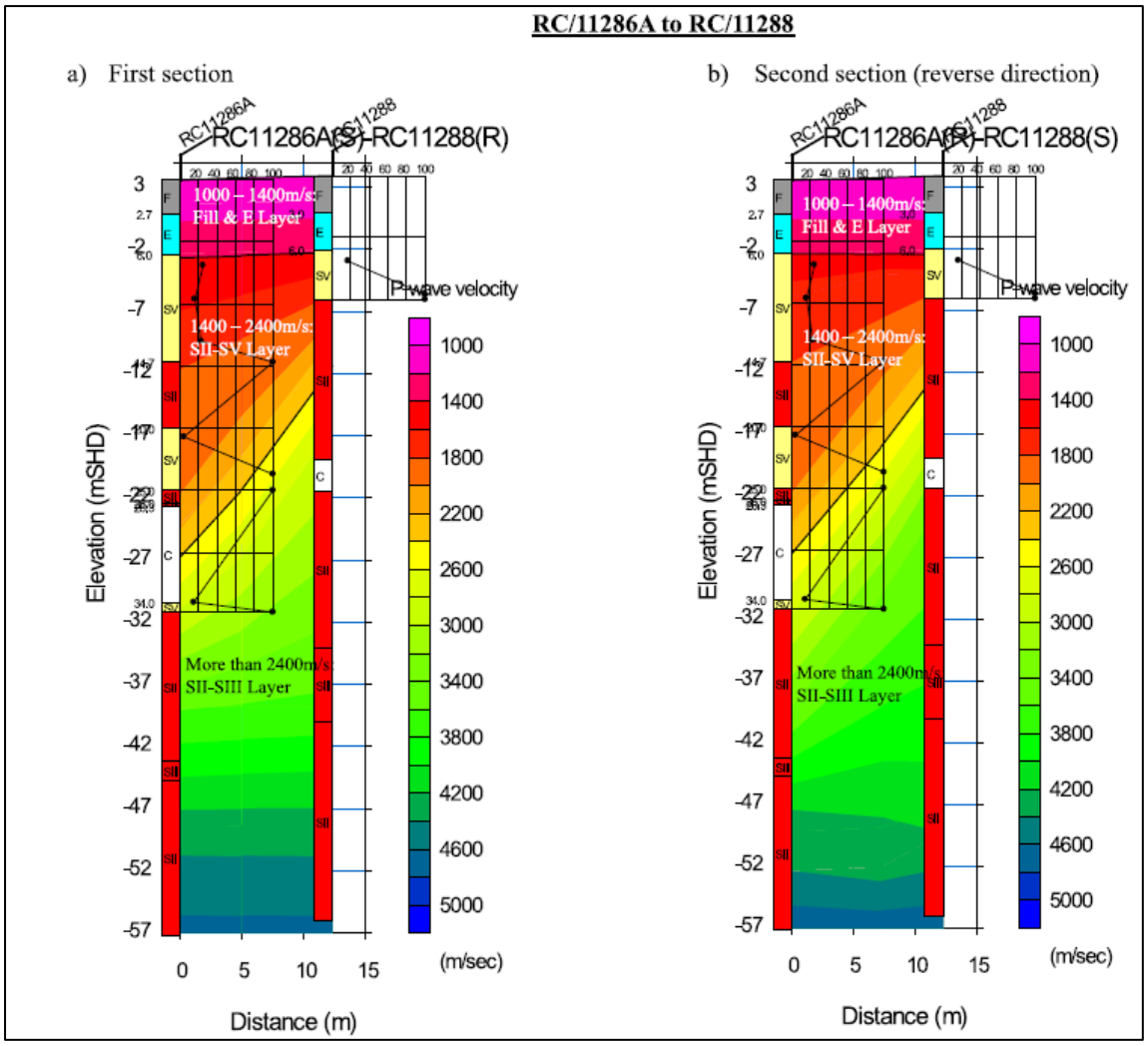

Figure 4.5 Crosshole Tomography results from RC/11286A to RC/11288 and vice versa

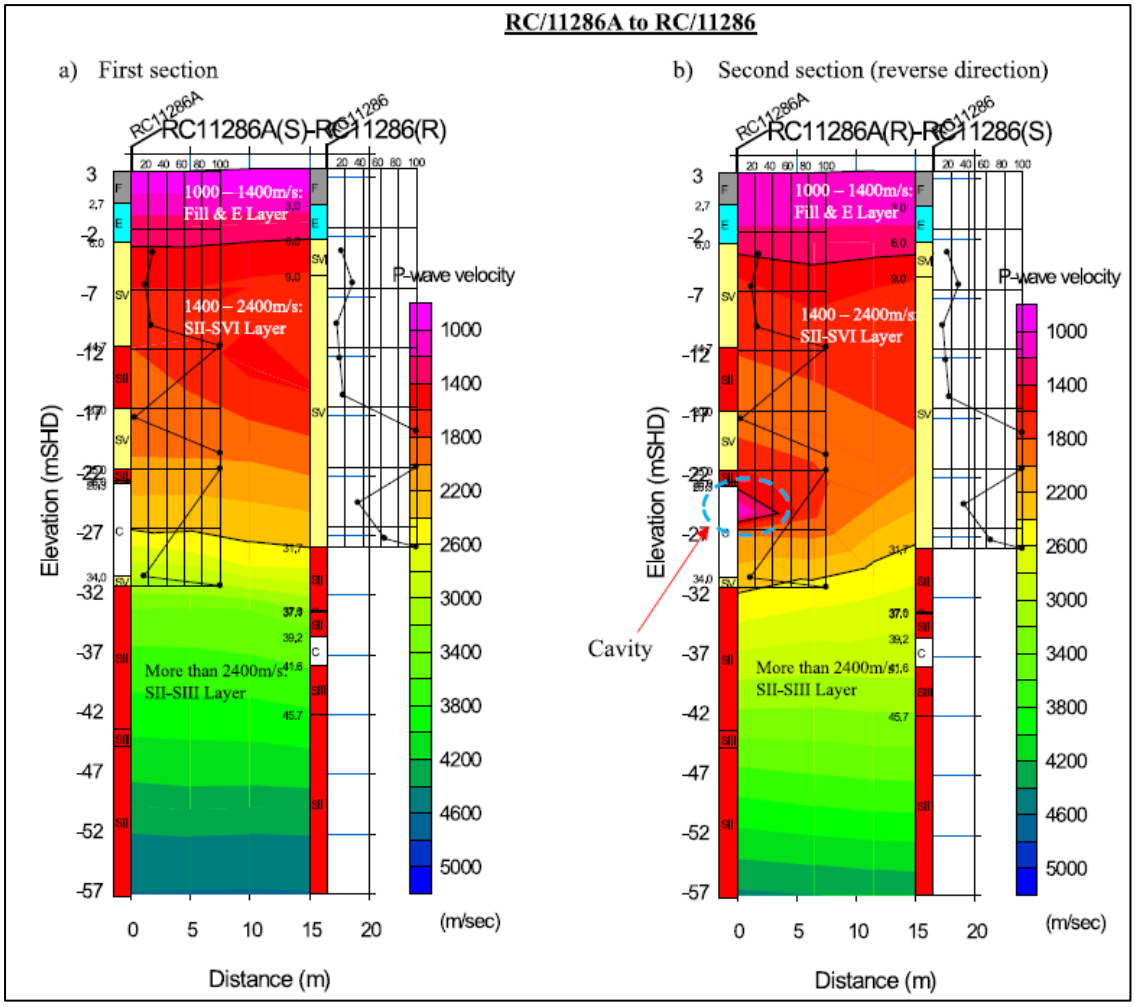

Figure 4.5 Crosshole Tomography results from RC/11286 to RC/11286A and vice versa

4.3 Microtremor

Microtremor survey was conducted along a straight line as shown in Figure 4.6. Figure 4.7 shows a cross-sectional profile along a survey line supplemented with data from three boreholes (RC/11286, RC/11286A, and RC/11288). The top 5 meters consist of firm to stiff fill and Kallang soil with shear wave velocities (Vs) around 200 m/s. Lower Vs values near the ends of the line are likely due to boundary effects. Beneath this, the profile transitions into weathered rock, with a central high-velocity zone (~500 m/s). A localized drop in Vs values was noted in between boreholes RC/11288 - RC/11286A and RC/11286A - RC/11286 and this coincides with the depths of the cavities as reported in the borehole logs.

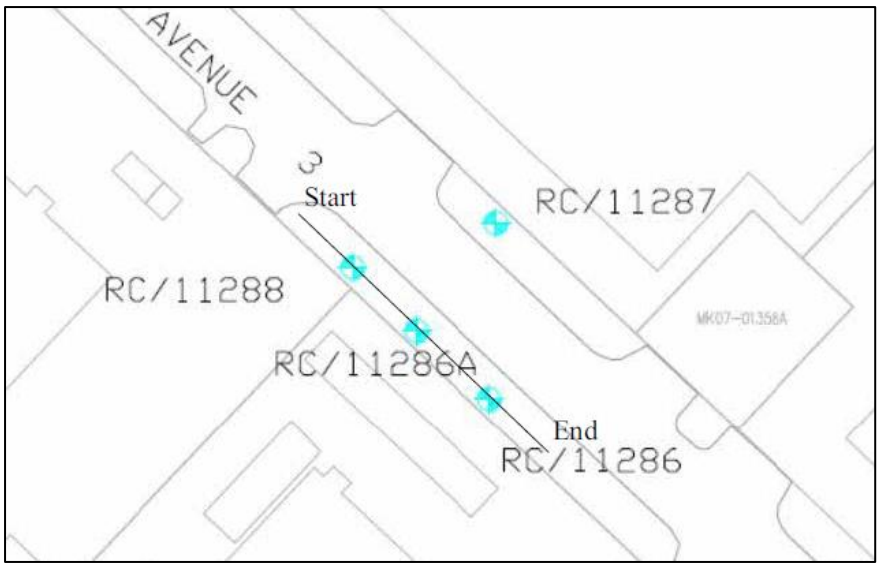

Figure 4.6 Layout plan of microtremor array line

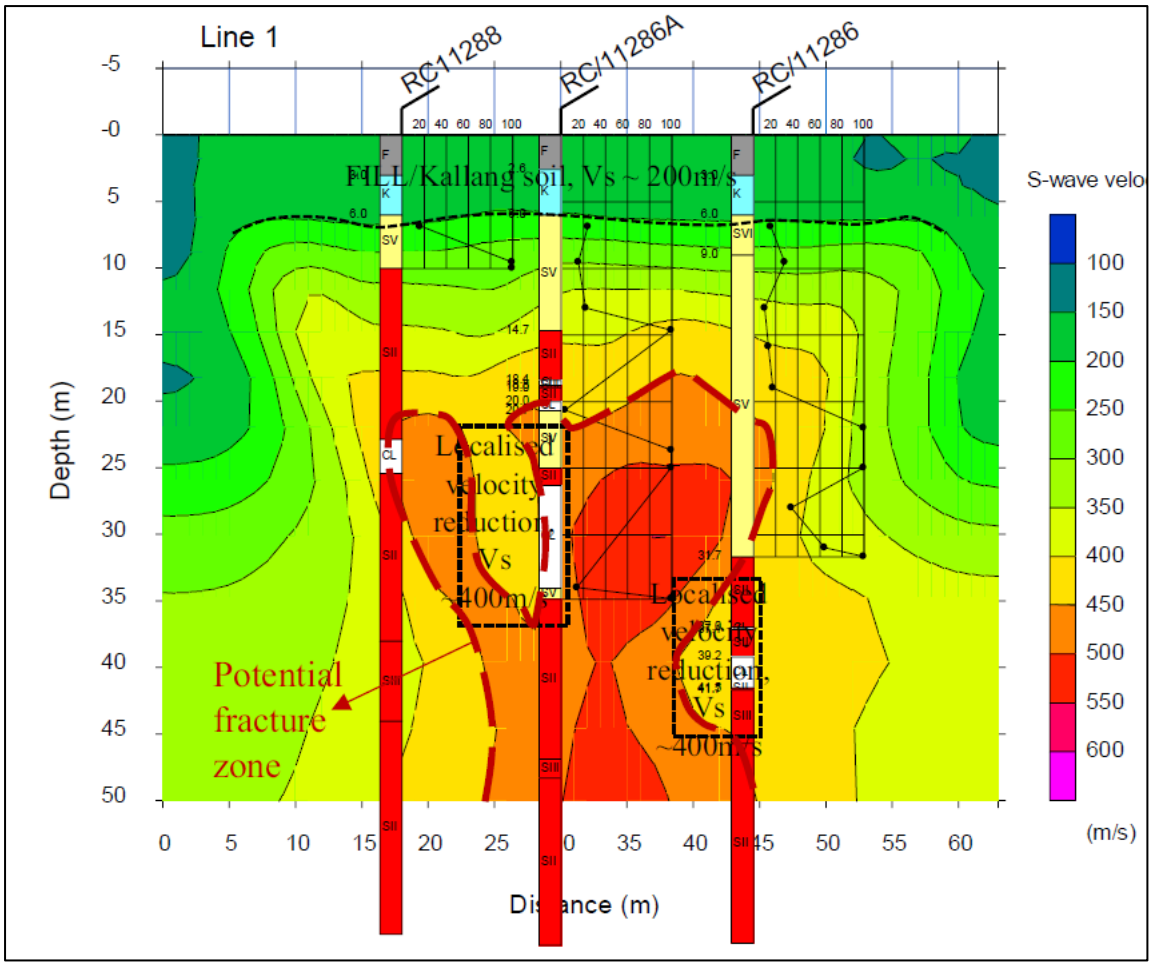

Figure 4.7 Microtremor Results S wave velocity longitudinal profile

4.4 Seismic Scattering

Seismic scattering was conducted along a straight line as shown in Figure 4.8 and conducted 1m away from borehole RC/11286A. The top 15m consist of Kallang formation till 6m and residual soil till 15m depth with P wave velocity of less than 700 m/s. After which, it transitions to weathered rock with P

wave velocity increasing from 700 m/s to 1300 m/s. Based on the results in Figure 4.10, it indicates a localized drop in P wave velocity approximately from depth 25m to 35m which coincides with the depth of the cavity in borehole RC/11286A. The exact depth of cavity as reported in the borehole log is from 26m to 34m (as shown in Figure 4.3).

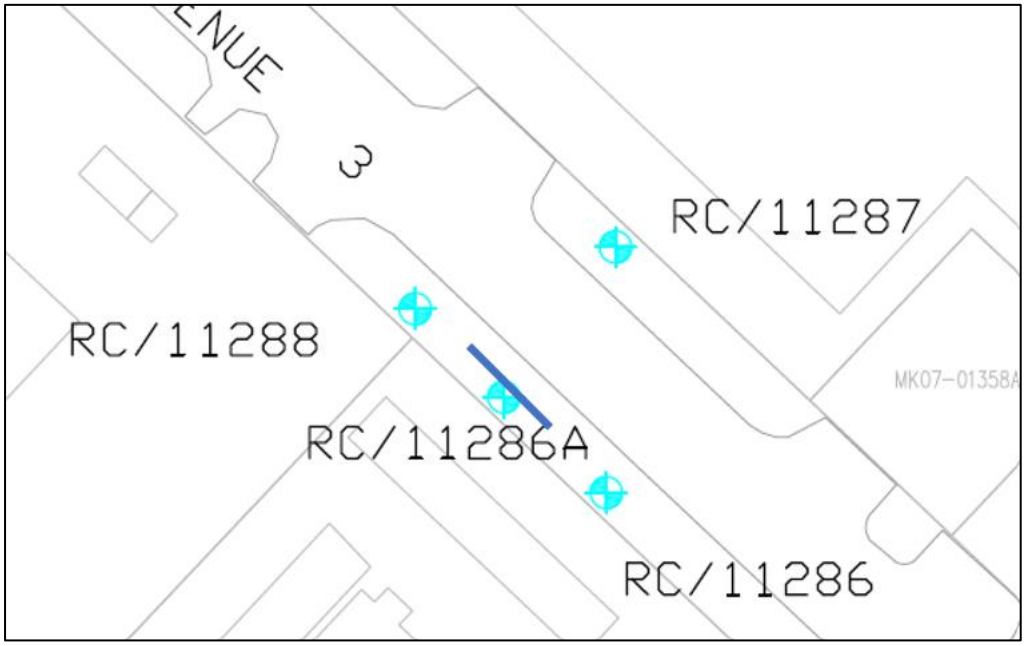

Figure 4.8 Layout plan of seismic scattering array line

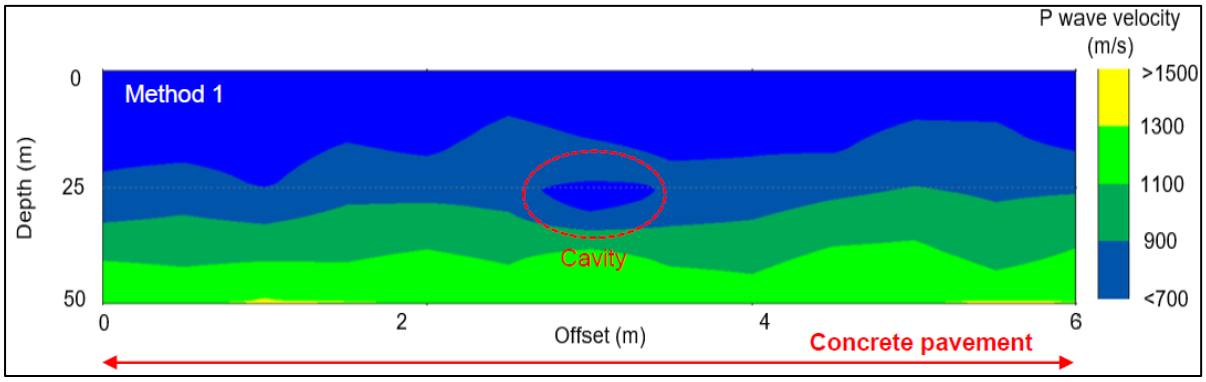

Figure 4.9 Seismic scattering P wave velocity profile

5. CONCLUSION

Various geophysical investigation techniques – including microgravity surveys, microtremor analysis, and seismic scattering – have demonstrated the capability to detect subsurface cavities. In contrast, cross-hole tomography did not reveal evidence of cavities, except for a localised anomaly identified in a single test; this outcome may be attributed to the specific shape and size of the cavities observed. Consequently, cross-hole tomography appears to be less suitable for identifying the types of cavities typically encountered in Singapore.

This study underscores that different geophysical methods exhibit varying effectiveness in cavity detection. It is therefore advisable to employ a combination of methods to more accurately determine cavity locations prior to conducting probe hole or borehole drilling. Integrating geophysical scanning with strategically targeted borehole drilling offers a cost-effective and reliable approach to cavity

identification for tunnelling projects. Given the extensive linear distance covered by tunnelling operations and the practical limitations of drilling boreholes at close intervals, relying solely on borehole drilling may overlook potential cavity sites. Accordingly, combining borehole drilling with preliminary geophysical scanning enhances the overall effectiveness of cavity detection efforts.

6. ACKNOWLEDGEMENT

The young author gratefully acknowledges the support and guidance provided by the senior co-author throughout the course of this study. The young author was responsible for reviewing and analysing the data while the co-author provided valuable insights, direction and actively stimulated critical thinking throughout the development of this study. Their collaborative efforts were instrumental in enhancing the depth and quality of the research.

7. REFERENCE

Rayleigh, "On waves propagated along the plane surface of an elastic solid", Proceedings of the London Mathematical Society, 1, pp. 4-11, 1985.

A.E.H. Love, "Mathematical theory of elasticity", Cambridge University Press, UK, 2013.

H. Lamb, "On the propagation of tremors over the surface of an elastic solid, Philosophical Transactions of the Royal Society of London. Series A", Containing papers of a mathematical or physical character, 203, pp. 1-42, 1904

Elhaj, Mohamed: Application of Gravity Survey for Geological Mapping and Cavity Detection: Malaysian Case Studies, 2015

Roman Krasnoperov, Roman Sidorov, Andrew Grudnev, Jon Karapetyan, Dmitry Lazarev: On the Magnetic Properties of Construction Materials for Magnetic Observatories, Appl. Sci. 2023, 13(4), 2246

Kornkanok Sangprasat,Avirut Puttiwongrak, Shinya Inazumi: Review of Correlations Between Soil Electrical Resistivity and Geotechnical Properties, Geosciences 2025, 15(5), 166

G. Coulouma, B. Tisseyre, P. Lagacherie, "Is a systematic two-dimensional EMI soil survey always relevant for vineyard produc-tion management? A test on two pedologically contrasting Medi-terranean vineyards", Proximal Soil Sensing, Springer, pp. 283-295, 2000

I. Bishop, P. Styles, S. Emsley, N. Ferguson, "The detection of cavities using the microgravity technique: case histories from mining and karstic environments", Geological Society, London, Engineering Geology Special Publications, 12, pp.153-166, 1997

William, C. P., Lee, L. M., & Michael, K. D. (1999). Reverse VSPs and Crosshole Seismic Tomography While Coring. SAGEEP (p. 997). Environmental & Engineering Geophysical Society.

Louis, I. F. (2001). Subsurface Imagingusing Crosshole Tomographic Techniques. Bulletin of Geological Society of Greece, Vol. XXXIV/4, 1371–1378.

Elin Asta Olafsdottir, Sigurdur Erlingsson, and Bjarni Bessason, Tool for analysis of multichannel analysis of surface waves (MASW) field data and evaluation of shear wave velocity profiles of soils, 2017

Revenaugh J (1999) Geological applications of seismic scattering. Annual Review of Earth and Planetary Sciences, 27, 55-73.

Kesar AS (2011) Underground anomaly detection by electromagnetic shock waves. IEEE Transactions on Antennas and Propagation, 59, 149-153.

Rappaport CM, Miller EL (1999) Physics-based modeling and inverse scattering for detection of buried mine-shaped anomalies. Proc. SPIE Subsurface Sensors and Applications, 3752.